Science Advances
AAAS

advances.sciencemag.org/cgi/content/full/6/3/eaay2174/DC1

Supplementary Materials for

Direct targeting of oncogenic RAS mutants with a tumor-specific cytosol-penetrating antibody inhibits RAS mutant–driven tumor growth

Seung-Min Shin, Ji-Sun Kim, Seong-Wook Park, Sei-Yong Jun, Hye-Jin Kweon, Dong-Ki Choi, Dakeun Lee, Yong Beom Cho, Yong-Sung Kim*

*Corresponding author. Email: kimys@ajou.ac.kr

Published 15 January 2020, *Sci. Adv.* **6**, eaay2174 (2020)
DOI: 10.1126/sciadv.aay2174

This PDF file includes:

fig. S1

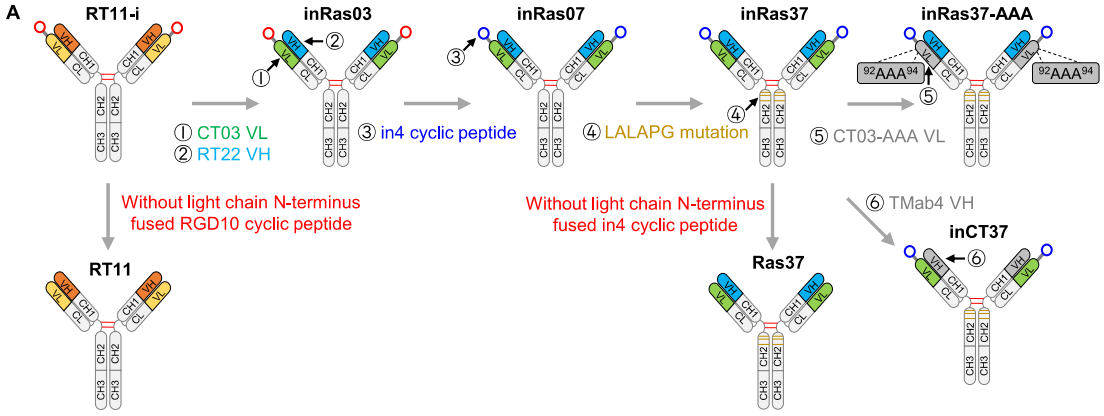

B

IgG Clones	VH	VL	Integrin αvβ5/αvβ3-targeting peptide	IgG1 Fc
RT11	RT11 VH	TMab4 VL	-	WT
RT11-i	RT11 VH	TMab4 VL	RGD10	WT
inRas03	RT22 VH	CT03 VL	RGD10	WT
inRas07	RT22 VH	CT03 VL	in4	WT
Ras37	RT22 VH	CT03 VL	-	LALAPG
inCT37	TMab4 VH	CT03 VL	in4	LALAPG
inRas37	RT22 VH	CT03 VL	in4	LALAPG
inRas37-AAA	RT22 VH	CT03-AAA VL	in4	LALAPG

Fig. S1. Procedures of stepwise engineering to generate the second-generation active RAS-specific iMab, inRas37. (**A**) A schematic representation of the stepwise engineering procedures to generate inRas37: i) RT11-i → inRas03: (1) The VL of RT11-i was replaced with the CT03 VL with enhanced endosomal-escape activity and improved developability by removing HSPG-binding activity; (2) The VH of RT11-i was replaced with the RT22 VH with enhanced affinity for the active RAS form. ii) inRas03 → inRas07: (3) the RGD10 cyclic peptide was replaced with affinity-matured integrin αvβ5-and-αvβ3–targeting cyclic peptide (called in4) for the receptor-mediated endocytosis. iii) inRas07 → inRas37: (4) LALAPG mutations (L234A, L235A, and P329G) were introduced into human IgG1 Fc to improve pharmacokinetics by abrogating interactions with FcγRs on immune cells.
We also generated control antibodies: inRas37-AAA, which has a substitution of ^{92}WYW^{94} with ^{92}AAA^{94} in the endosomal-escape motif of the CT03 VL (5) such that it has no endosome-escape activity; inCT37, which has the null VH of TMab4 without RAS-binding activity (6) such that it does not bind to RAS; RT11 and RAS37, which have no light chain N-terminus-fused integrin-targeting cyclic peptide. (**B**) The summary of functional components (VH, VL, the integrin αvβ5-and-αvβ3–targeting cyclic peptide, and Fc regions) of active RAS-targeting iMabs and control antibodies used in this study.

fig. S2

A

	VH-CDR1						VH-CDR2																VH-CDR3								
Kabat No.	31	32	33	34	35		50	51	52	52a	53	54	55	56	57	58	59	60	61	62	63	64	65		95	96	97	98	99	100	100a	101	102
RT11 VH	S	Y	S	M	S		Y	I	S	R	T	S	H	T	T	Y	Y	A	D	S	V	K	G		G	F	F				M	D	Y
RT22 VH	D	F	·	·	·		·	·	·	·	·	·	·	·	·	·	·	·	·	·	·	·	·		·	·	K				·	·	·

B

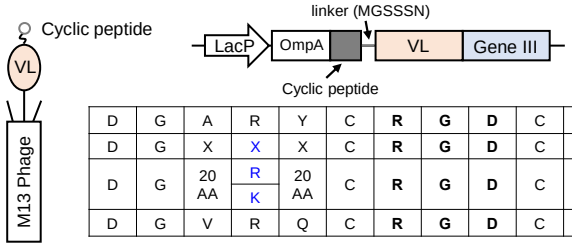

D	G	A	R	Y	C	**R**	**G**	**D**	C	F	D	G			**RGD10 cyclic peptide**
D	G	X	X	X	C	**R**	**G**	**D**	C	X	X	X	X	X	
D	G	20 AA	R / K	20 AA	C	**R**	**G**	**D**	C	20 AA	D / E	20 AA	20 AA	20 AA	**RGD Library**
D	G	V	R	Q	C	**R**	**G**	**D**	C	F	D	G	P	L	**in4 cyclic peptide**

C

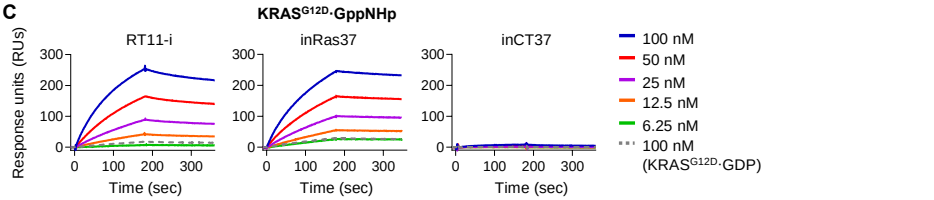

D

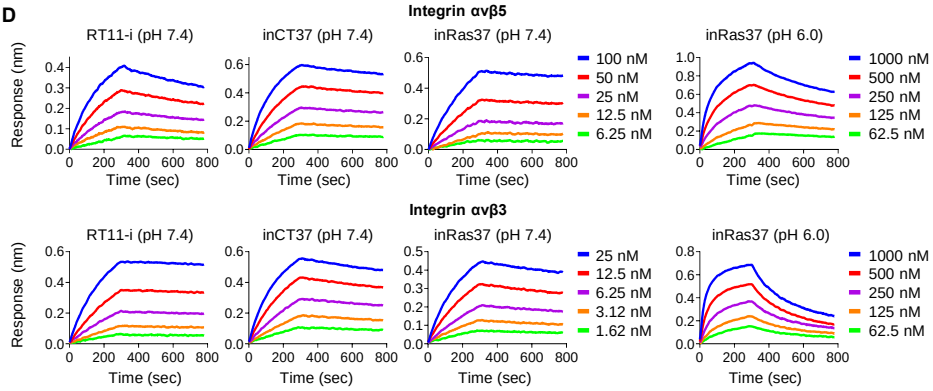

E

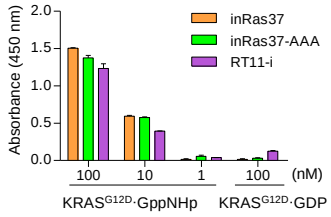

Fig. S2. Preparation of the RT22 VH and in4 cyclic peptide and biochemical characterization of inRas37. (**A**) Amino acid sequence alignment of the active RAS-specific RT11 VH and RT22 VH. The RT22 VH was isolated from a yeast surface-displayed library with randomization in VH-CDR1 and VH-CDR3 of the RT11 VH in single-chain Fab format by pairing with a fixed LC (CT03 VL-Cκ) and then screening it against the biotinylated GppNHp-loaded $KRAS^{G12D}$·($KRAS^{G12D}$·GppNHp) active form in the presence of a 10-fold molar excess of the nonbiotinylated GDP-loaded $KRAS^{G12D}$ ($KRAS^{G12D}$·GDP) inactive form as a soluble competitor. (**B**) The phage library construction scheme and sequence of the isolated in4 cyclic peptide. The phage library of the RGD10 cyclic peptide was generated with randomization on the "X"-denoted residues with degenerate codons of NNK (20 aa), ARR (R or K), and GAN (D or E) as a fusion to the N-terminus of the CT03 VL and then screened against integrin αvβ5, thus yielding the in4 cyclic peptide. (**C**) Representative SPR sensorgrams showing the kinetic interactions of RT11-i, inRas37, and inCT37 with active $KRAS^{G12D}$·GppNHp, whose concentrations are indicated (colored). The injection of $KRAS^{G12D}$·GDP (100 nM) (dashed line) yielded negligible binding to RT11-i and inRas37. (**D**) Representative binding isotherms of the immobilized antibodies to a soluble antigen, integrin αvβ5 and αvβ3, as measured at the indicated pH by biolayer interferometry on the Octet QKe system (ForteBio). The concentrations of integrin αvβ5 and αvβ3 are indicated (colored). (**E**) Binding activity of inRas37, inRas37-AAA, and RT11-i toward $KRAS^{G12D}$·GppNHp or $KRAS^{G12D}$·GDP, as determined by an ELISA. Error bars represent the mean ± SD (n = 3).

fig. S3

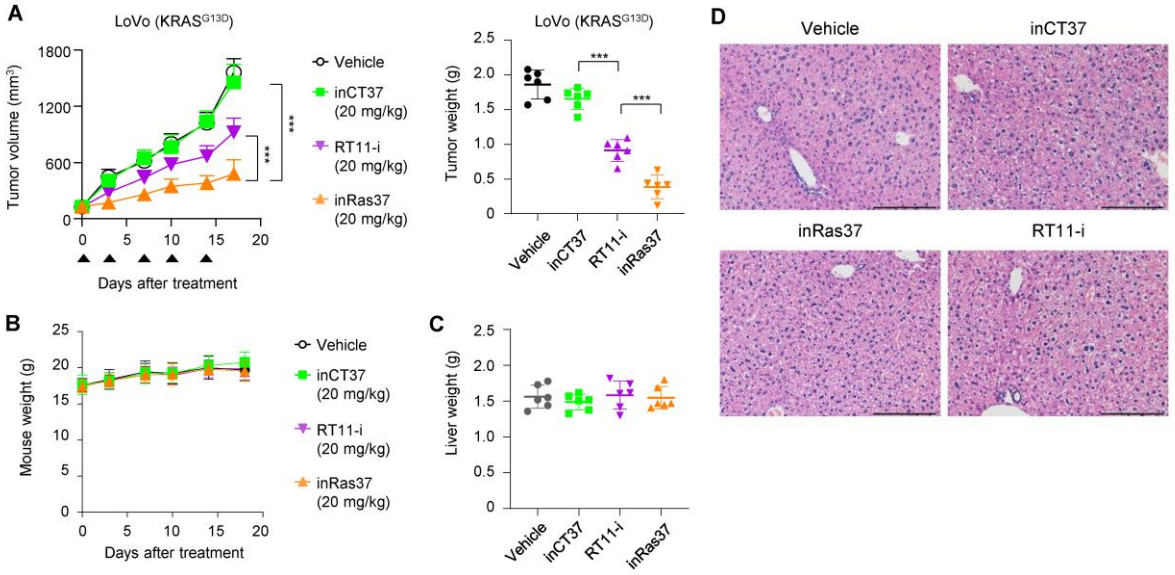

Fig. S3. inRas37 has more potent antitumor efficacy in vivo than RT11-i does, without noticeable toxic side effects. (A) Tumor growth curves measured during treatment (left) and tumor weight at the end of treatment (right) in response to i.v. injection of the indicated antibodies twice a week (arrows) at a dose of 20 mpk for a total 5 doses into BALB/c nude mice harboring LoVo tumor xenografts. (**B**) Mouse body weight measured during the treatments as described in (**A**). (**C**) Liver weights of mice after treatment as described in (**A**). (**D**) Hematoxylin and eosin (H&E) staining of representative tissue slides from the liver of mice after treatment as described in (**A**). Abnormal histological features suggestive of hepatic toxicity, e.g., hepatocyte degeneration, necrosis, fat content change, cholestasis, portal/periportal inflammation, and fibrosis, were not observed in all samples. Magnification, ×200; scale bar, 100 μm. In (**A**-**C**), error bars represent the mean ± SD (n = 6 per group). ****P* < 0.001 between the indicated groups.

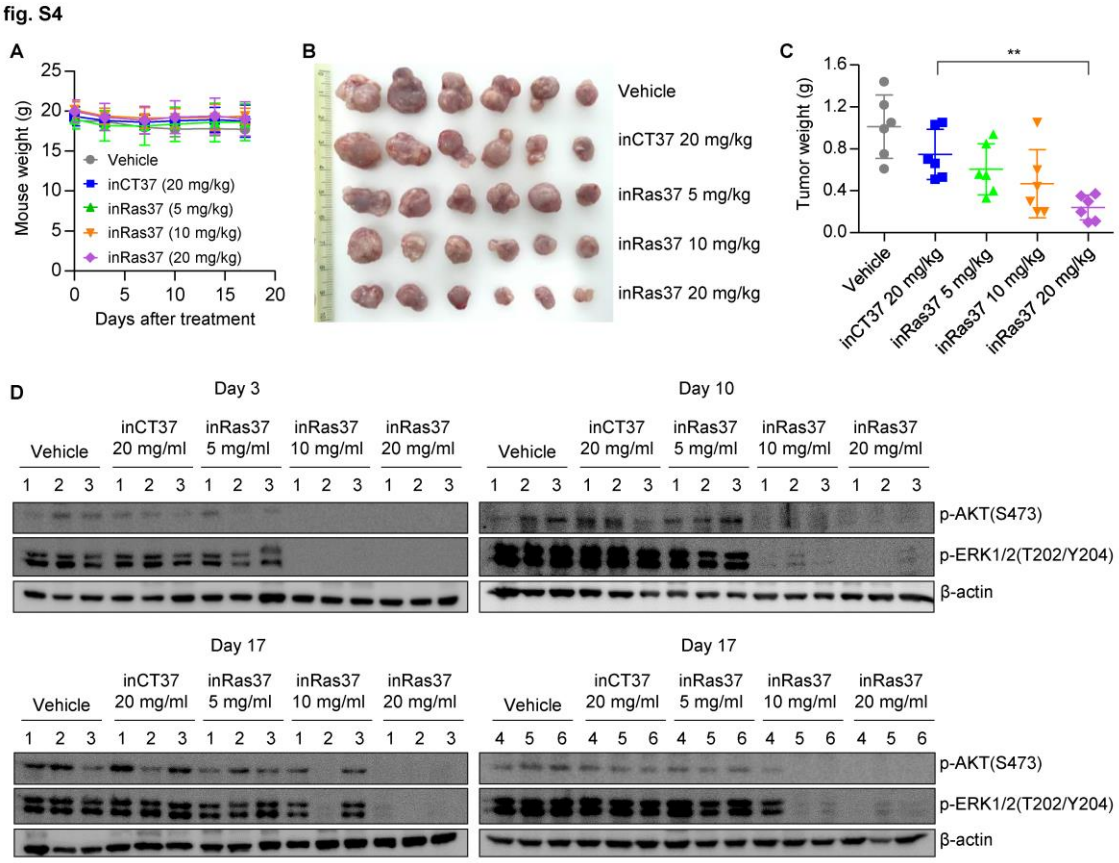

Fig. S4. inRas37 causes dose-dependent inhibition of in vivo growth of KRAS^{G12V} SW480 tumor xenografts in mice. (**A**) Mouse body weight measured during the treatments described in Fig. 4B. Error bars represent the mean ± SD (n = 6 per group). (**B**) Photographs of tumors excised from mice after the treatment described in Fig. 4B. (**C**) The weight of individual tumors from each treatment group. Error bars represent the mean ± SD (n = 6 per group). Statistical analyses were performed by one-way ANOVA followed by the Newman–Keuls *post hoc* test. ***P* < 0.01 vs. group inCT37. (**D**) Western blot analysis of p-ERK1/2 and p-AKT in tumor tissue lysates prepared before antibody dosing on days 3 and 10 and at the end of treatment on day 17 (n = 3 per group on days 3 and 10, n = 6 per group on day 17). The quantified data are given in Fig 4D. All images are representative of at least two independent experiments.

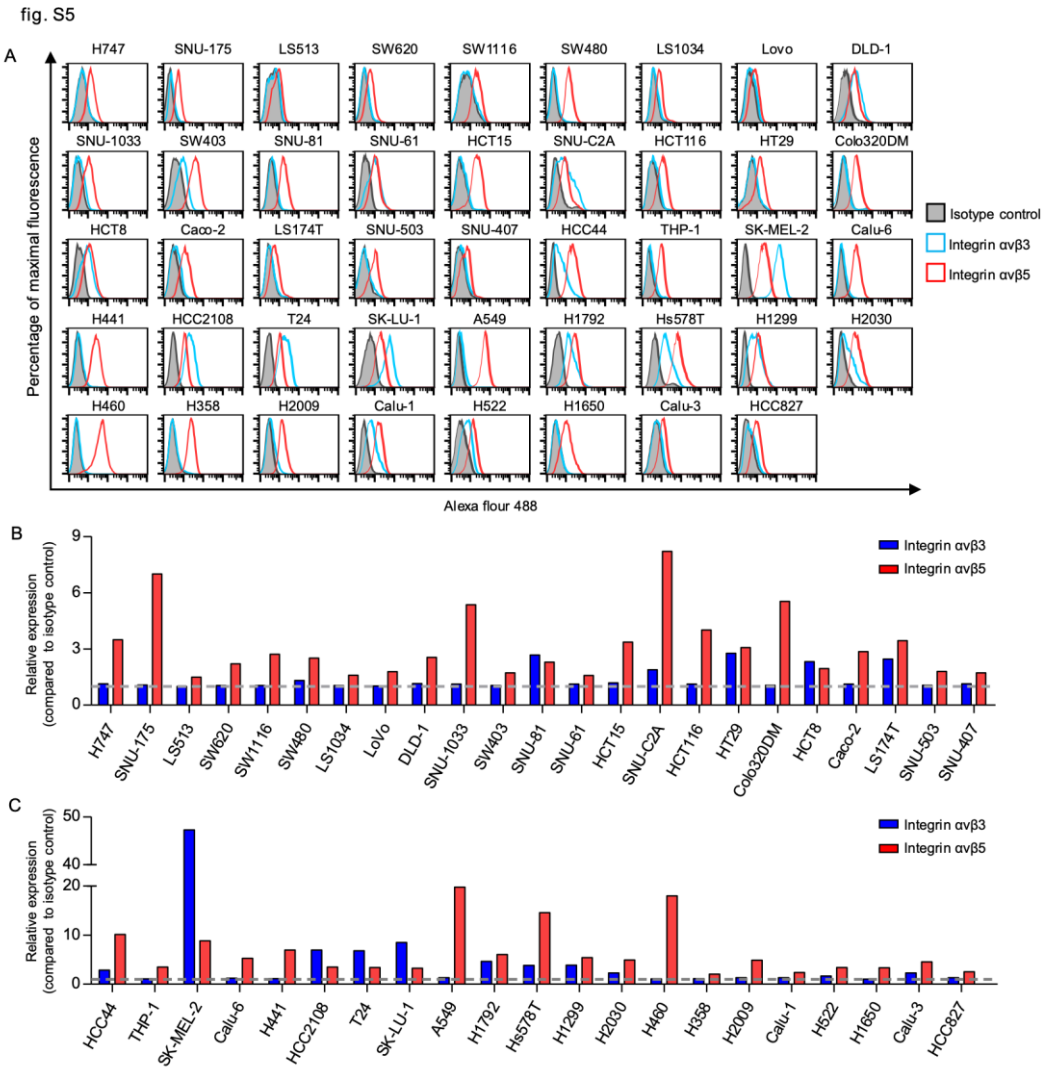

Fig. S5. Comparison of cell surface expression levels of integrin αvβ5 and integrin αvβ3 in various RAS^{WT} and RAS^{MUT} cell lines. (**A**) Flow-cytometric analysis of cell surface expression levels of integrin αvβ3 and integrin αvβ5 in various RAS^{MUT} and RAS^{WT} cell lines used in Fig. 5A. (**B** and **C**) Relative expression of cell surface integrin αvβ3 and integrin αvβ5 compared to isotype control in colorectal cancer (**B**), lung cancer, melanoma, bladder cancer, acute monocytic leukemia, and breast cancer cells (**C**). Mean fluorescence intensity (MFI) values were determined in the FlowJo software, and relative expression levels were calculated as follows: relative expression = (MFI of anti-integrin αvβ3 or αvβ5 antibody)/(MFI of isotype control antibody). The horizontal dotted lines indicate the relative expression = 1.0.

fig. S6

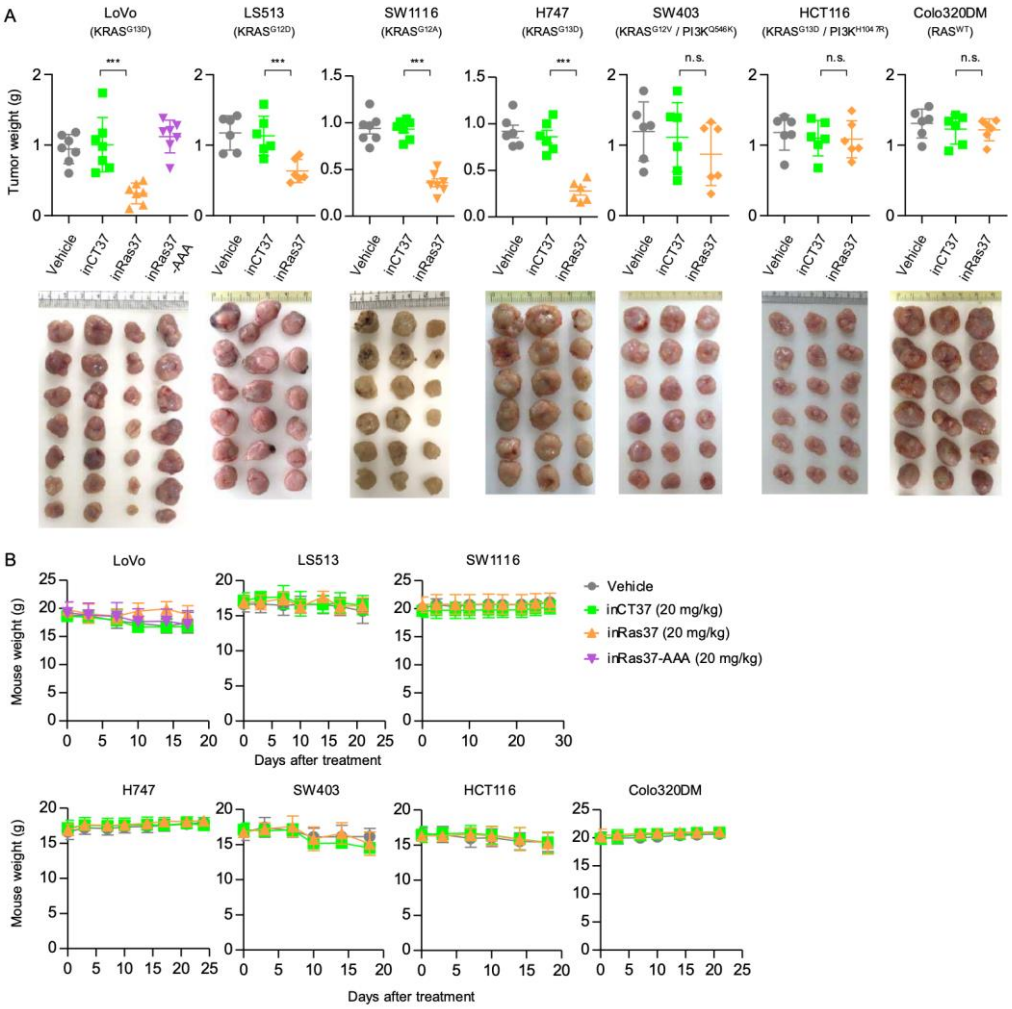

Fig. S6. inRas37 suppresses the in vivo growth of various RAS^{MUT} tumor xenografts in mice without noticeable systemic toxicity. (**A**) The weight of individual tumors from each treatment group (upper panels) and photographs of tumors (lower panels) excised from mice 24 h after last treatment, as shown Fig. 5C. Statistical analyses were performed by one-way ANOVA followed by the Newman–Keuls *post hoc* test. ***$P < 0.01$ vs. group inCT37; n.s., not significant. (**B**) Mouse body weight measured during the treatments described in Fig. 5C. In (**A**, **B**), error bars represent the mean ± SD (n = 6 per group, except for LoVo, n = 7 per group).

fig. S7

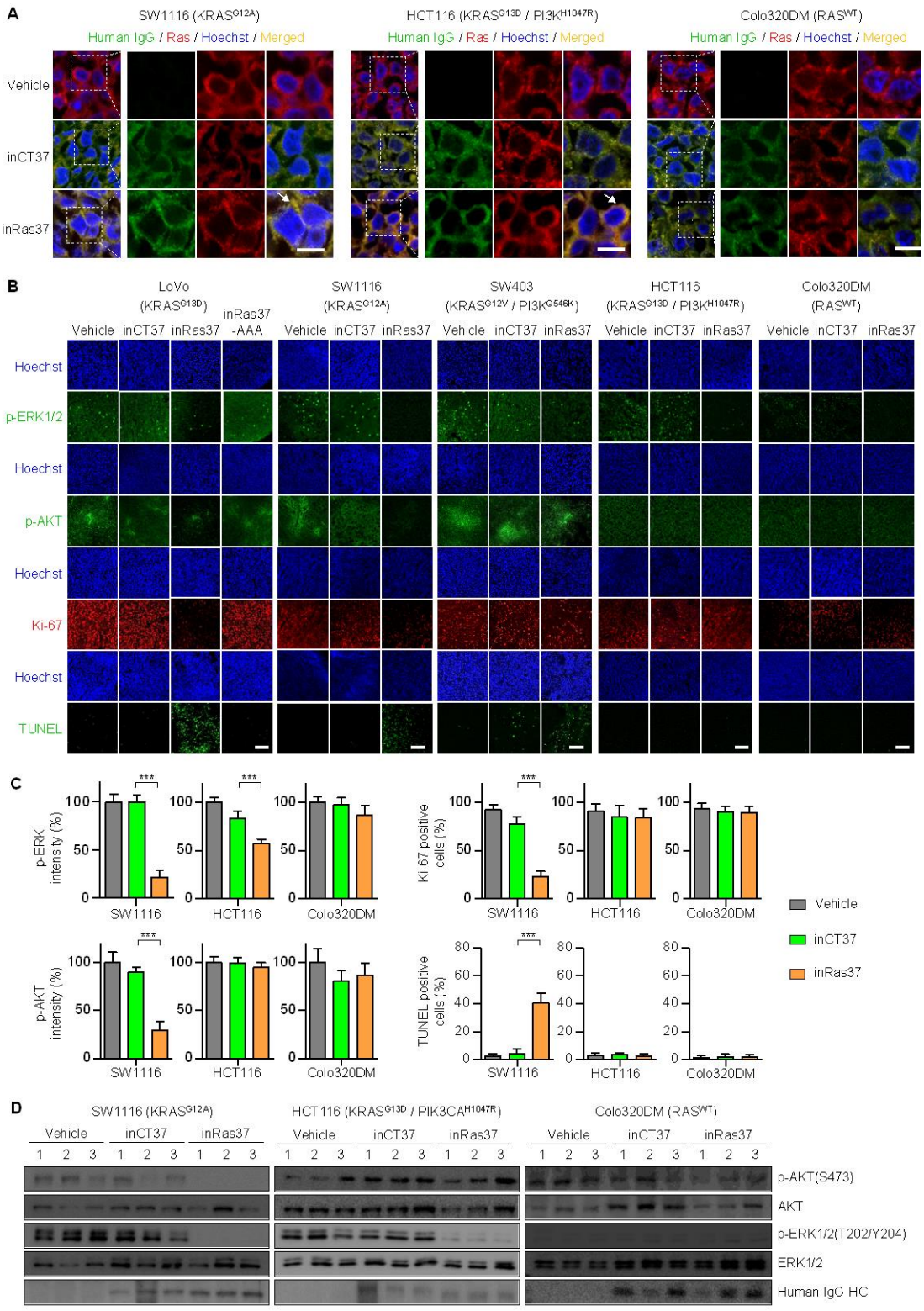
A
SW1116 (KRASG12A)
HCT116 (KRASG13D / PI3KH1047R)
Colo320DM (RASWT)
Human IgG / Ras / Hoechst / Merged
Vehicle
inCT37
inRas37
B
LoVo (KRASG13D)
SW1116 (KRASG12A)
SW403 (KRASG12V / PI3KQ546K)
HCT116 (KRASG13D / PI3KH1047R)
Colo320DM (RASWT)
Vehicle inCT37 inRas37 inRas37 -AAA
Hoechst
p-ERK1/2
p-AKT
Ki-67
TUNEL
C
p-ERK intensity (%)
Ki-67 positive cells (%)
p-AKT intensity (%)
TUNEL positive cells (%)
SW1116
HCT116
Colo320DM
Vehicle
inCT37
inRas37
D
SW1116 (KRASG12A)
HCT116 (KRASG13D / PIK3CAH1047R)
Colo320DM (RASWT)
p-AKT(S473)
AKT
p-ERK1/2(T202/Y204)
ERK1/2
Human IgG HC

Fig. S7. IHC and Western blot analyses of tumor tissues excised from mice after treatment. (**A**) IHC analysis of the indicated antibodies (green), with activated RAS (red) in SW1116-, HCT116-, and Colo320DM-derived tumor tissues prepared 24 h after last treatment. The arrows indicate the colocalization of inRas37 with activated RAS. Scale bar, 10 μm. (**B**) IHC analysis of p-ERK1/2 (green), p-AKT (green), Ki-67 (red), and TUNEL (green) staining levels in LoVo-, SW403-, SW1116-, HCT116-, and Colo320DM-derived tumor tissues prepared 24 h after last treatment. Scale bar, 100 μm. The quantified data are shown in Fig. 5E. (**C**) The relative fluorescence intensity (%) compared to that in the vehicle-treated control and the percentage of Ki-67–positive and TUNEL-positive cells as compared to the number of Hoechst 33342–stained cells for each sample. Error bars represent the mean ± SD of five random fields for each immunofluorescent sample (n = two tumors per group). Statistical analyses were performed by one-way ANOVA followed by the Newman–Keuls *post hoc* test. ***$P < 0.001$ *vs*. inCT37. (**D**) Western blot analysis of the indicated proteins in SW1116-, HCT116-, and Colo320DM-derived tumor tissue lysates prepared 24 h after the last treatment. All images are representative of at least two independent experiments.

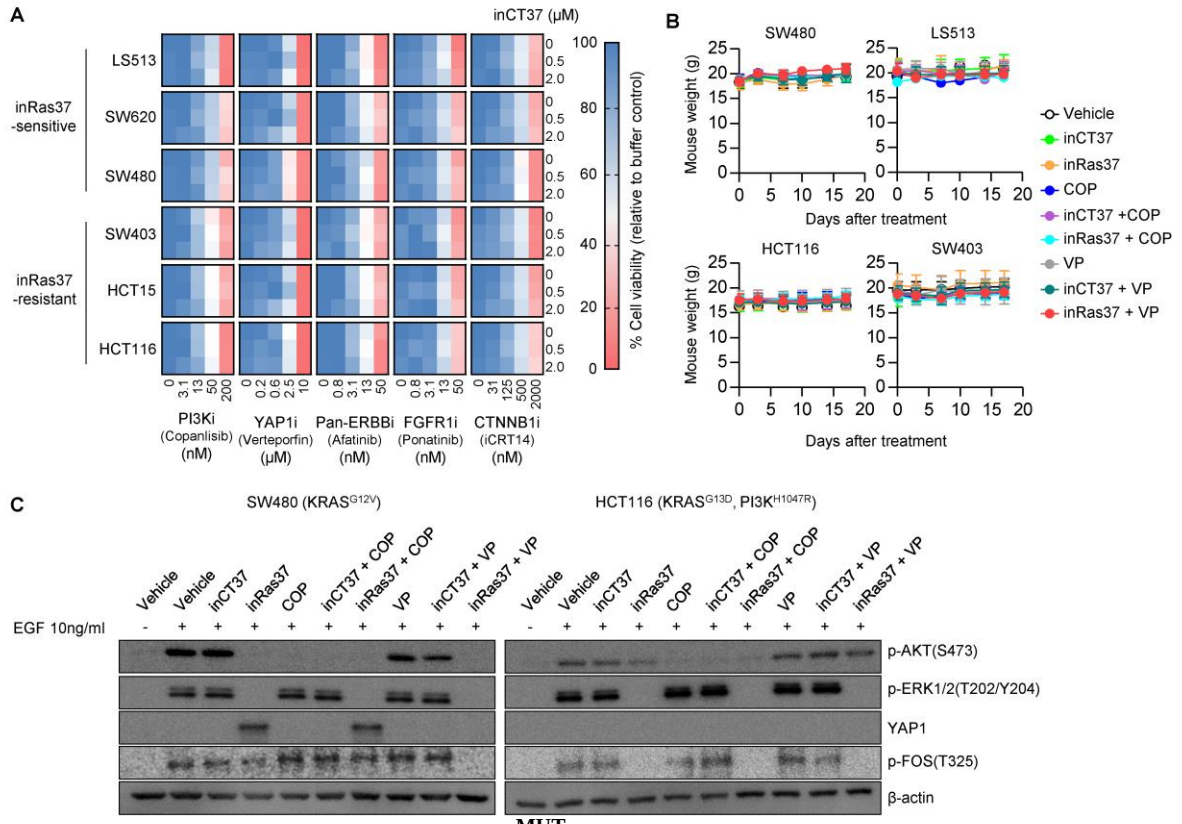

Fig. S8. Combined treatment of KRAS^{MUT} cell lines with a pharmacological inhibitor and either inRas37 or inCT37. (**A**) Dose–response effects of combined treatment with inCT37 and one of five pharmacological inhibitors ("i" in the label) on the viability of KRAS^{MUT} cancer cells after combined treatment every other day (days 0, 2, and 4) at the indicated concentrations for 6 d in 3D-spheroid cultures. Heatmaps indicate percentages of cell viability relative to buffer-treated control (n = 3). The combinations of inCT37 with one of the five pharmacological inhibitors did not show any synergistic effects. (**B**) Mouse body weight measured during the treatments described in Fig. 6C. Error bars represent the mean ± SD (n = 6 per group). (**C**) Western blot analysis of the indicated proteins in inRas37-sensitive SW480 cells and inRas37-resistant HCT116 cells, treated twice, at 0 and 48 h, with the indicated antibodies (2 μM), VP (YAP1i verteporfin, 2.5 μM), or COP (PI3Ki copanlisib, 50 nM) alone or as the indicated combination for 54 h in media containing of 1% FBS and then were stimulated with EGF (10 ng/ml) for 10 min before cell lysis. All images are representative of at least two independent experiments. These *in vitro* experiments suggested that YAP1 overexpression represents activation of an adaptive parallel signaling pathway to counteract the KRAS^{MUT}-blocking effect of inRas37 only in inRas37-sensitive cell lines, as shown in the *in vivo* experiments. The adaptive resistance was overcome by a combination of inRas37 and VP (YAP1i verteporfin).

Table S1. Binding constants for the interactions of inRas37 with GppNHp-loaded active forms of RAS, as determined by SPR analysis.

Anti-bodies	RAS proteins	Kinetic parameters*		
		k_a ($M^{-1} s^{-1}$)	k_d (s^{-1})	K_D (M)
RT11-i	$KRAS^{G12D}$·GppNHp	$(1.99 \pm 0.81) \times 10^{4}$	$(2.82 \pm 1.51) \times 10^{-4}$	$(1.42 \pm 1.13) \times 10^{-8}$
inRas37	$KRAS^{WT}$·GppNHp	$(3.64 \pm 0.27) \times 10^{4}$	$(2.69 \pm 0.56) \times 10^{-4}$	$(7.47 \pm 1.90) \times 10^{-9}$
	$KRAS^{G12D}$·GppNHp	$(8.19 \pm 0.30) \times 10^{4}$	$(5.87 \pm 0.40) \times 10^{-4}$	$(7.17 \pm 0.52) \times 10^{-9}$
	$KRAS^{G12V}$·GppNHp	$(3.28 \pm 0.29) \times 10^{4}$	$(3.06 \pm 0.29) \times 10^{-4}$	$(9.42 \pm 1.69) \times 10^{-9}$
	$KRAS^{G13D}$·GppNHp	$(5.26 \pm 0.26) \times 10^{4}$	$(4.84 \pm 0.09) \times 10^{-4}$	$(9.21 \pm 0.41) \times 10^{-9}$
	$KRAS^{Q61H}$·GppNHp	$(5.68 \pm 0.57) \times 10^{4}$	$(4.92 \pm 0.21) \times 10^{-4}$	$(8.69 \pm 0.49) \times 10^{-9}$
	$HRAS^{WT}$·GppNHp	$(4.19 \pm 1.16) \times 10^{5}$	$(3.30 \pm 1.04) \times 10^{-3}$	$(7.81 \pm 0.55) \times 10^{-9}$
	$HRAS^{G12V}$·GppNHp	$(3.79 \pm 0.27) \times 10^{4}$	$(1.72 \pm 0.38) \times 10^{-4}$	$(4.52 \pm 0.78) \times 10^{-9}$
	$NRAS^{WT}$·GppNHp	$(3.30 \pm 0.49) \times 10^{4}$	$(2.78 \pm 0.28) \times 10^{-4}$	$(8.50 \pm 0.99) \times 10^{-9}$
	$NRAS^{Q61R}$·GppNHp	$(5.86 \pm 0.75) \times 10^{5}$	$(7.50 \pm 0.58) \times 10^{-3}$	$(1.21 \pm 0.08) \times 10^{-8}$

* Each value represents the mean ± SD of two independent experiments. In each experiment, at least five datasets were used to determine the kinetic constants. The dissociation (k_{off}) and association rate constants (k_{on}) and the dissociation equilibrium constant (K_D) values, were determined via the 1:1 Langmuir binding model in the BIAevaluation software.

Table S2. Binding constants for the interactions of inRas37 with integrin αvβ5 and integrin αvβ3, as determined at pH 7.4 and/or pH 6.0 by biolayer interferometry.

Integrin proteins	Antibodies	pH	Kinetic parameters*		
			k_a ($M^{-1}s^{-1}$)	k_d (s^{-1})	K_D (M)
Integrin αvβ5	RT11-i	pH 7.4	$(6.73 \pm 0.08) \times 10^{4}$	$(4.69 \pm 0.03) \times 10^{-4}$	$(7.04 \pm 0.10) \times 10^{-9}$
	inCT37	pH 7.4	$(7.58 \pm 0.07) \times 10^{4}$	$(2.37 \pm 0.02) \times 10^{-4}$	$(3.13 \pm 0.04) \times 10^{-9}$
	inRas37	pH 7.4	$(3.77 \pm 0.05) \times 10^{4}$	$(1.55 \pm 0.05) \times 10^{-4}$	$(4.10 \pm 0.14) \times 10^{-9}$
		pH 6.0	$(1.52 \pm 0.02) \times 10^{4}$	$(8.13 \pm 0.14) \times 10^{-4}$	$(5.33 \pm 0.13) \times 10^{-8}$
Integrin αvβ3	RT11-i	pH 7.4	$(2.07 \pm 0.02) \times 10^{5}$	$(9.40 \pm 0.20) \times 10^{-5}$	$(4.53 \pm 0.11) \times 10^{-10}$
	inCT37	pH 7.4	$(2.71 \pm 0.03) \times 10^{5}$	$(3.01 \pm 0.02) \times 10^{-4}$	$(1.11 \pm 0.01) \times 10^{-9}$
	inRas37	pH 7.4	$(4.36 \pm 0.06) \times 10^{5}$	$(1.88 \pm 0.01) \times 10^{-3}$	$(4.30 \pm 0.06) \times 10^{-9}$
		pH 6.0	$(2.94 \pm 0.06) \times 10^{4}$	$(2.55 \pm 0.02) \times 10^{-3}$	$(8.66 \pm 0.20) \times 10^{-8}$

* Each value represents the mean ± SE of two independent experiments. In each experiment, at least five datasets were used to determine the kinetic constants. The dissociation (k_{off}) and association rate constants (k_{on}) and the dissociation equilibrium constant (K_D) values were determined by means of the 1:1 Langmuir binding model in the ForteBio Octet data analysis software (version 11.0).

Table S3. Quantitative assessment of the cellular uptake and cytosolic concentrations of RT11-i and inRas37 in HeLa and SW480 cells.

Parameters from quantitative western blotting assay in HeLa cell line [*]						
	RT11-i concentration (μM)			inRas37 concentration (μM)		
	0.1	0.5	1	0.1	0.5	1
Antibody in culture media at time point = 0 h (***T***) (pmole)	39.9 ± 0.9	193 ± 3	348 ± 4	38.7 ± 1.1	168 ± 6	336 ± 10
Antibody in culture media after 6 h incubation (***R***) (pmole)	36.0 ± 0.6	178 ± 5	326 ± 4	36.4 ± 0.9	160 ± 4	323 ± 11
Internalized amount of Antibody (***I***) (pmole) [†]	0.25 ± 0.02	0.67 ± 0.06	1.03 ± 0.07	0.18 ± 0.02	0.49 ± 0.05	0.75 ± 0.06
Cellular uptake efficiency (%) =[***I*** + (***T***-(***R***+***I***))]/***T***×100 [†]	8.56 ± 1.09	7.58 ± 2.12	5.92 ± 1.98	5.94 ± 1.71	4.49 ± 1.81	3.96 ± 1.14
Intracellular concentration of antibody (μM) [‡]	0.63 ± 0.03	1.68 ± 0.05	2.58 ± 0.05	0.45 ± 0.02	1.23 ± 0.03	1.88 ± 0.05
Parameters from split GFP complementation assay in HeLa-SA-GFP1-10 cell line [§]						
	RT11-i concentration (μM)			inRas37 concentration (μM)		
	0.1	0.5	1	0.1	0.5	1
Cytosolic amount of antibody (fmole)	0.41 ± 0.09	2.63 ± 0.27	5.82 ± 0.49	0.59 ± 0.25	5.28 ± 0.43	12.0 ± 0.66
Cytosolic concentration of antibody (nM) [‖]	18 ± 5	116 ± 12	258 ± 19	26 ± 11	234 ± 17	531 ± 24
Endosome-escape efficiency (%) [¶]	1.6 ± 0.5	3.9 ± 0.8	5.7 ± 0.1	3.4 ± 1.0	10.8 ± 0.2	16.0 ± 1.9
Parameters from quantitative western blotting assay in SW480 cell line [*]						
	RT11-i concentration (μM)			inRas37 concentration (μM)		
	0.1	0.5	1	0.1	0.5	1
Antibody in culture media at time point = 0 h (***T***) (pmole)	42.7 ± 0.7	163 ± 5	348 ± 9	40.5 ± 1.2	200 ± 7	362 ± 11
Antibody in culture media after 6 h incubation (***R***) (pmole)	39.7 ± 0.5	158 ± 7	333 ± 8	38.7 ± 0.7	190 ± 6	349 ± 10
Internalized amount of Antibody (***I***) (pmole) [†]	0.10 ± 0.01	0.29 ± 0.04	0.57 ± 0.07	0.06 ± 0.02	0.32 ± 0.05	0.40 ± 0.05
Cellular uptake efficiency (%) =[***I*** + (***T***-(***R***+***I***))]/***T***×100 [†]	6.96 ± 0.64	4.21 ± 0.59	4.08 ± 0.51	4.95 ± 1.13	4.42 ± 0.95	3.38 ± 0.79
Intracellular concentration of antibody (μM) [‡]	0.30 ± 0.02	0.73 ± 0.05	1.43 ± 0.06	0.20 ± 0.02	0.80 ± 0.05	1.03 ± 0.10
Parameters from split GFP complementation assay in SW480-SA-GFP1-10 cell line [§]						
	RT11-i concentration (μM)			inRas37 concentration (μM)		
	0.1	0.5	1	0.1	0.5	1
Cytosolic amount of antibody (fmole)	0.17 ± 0.07	1.12 ± 0.16	2.48 ± 0.36	0.25 ± 0.18	2.25 ± 0.14	5.11 ± 0.57
Cytosolic concentration of antibody (nM) [‖]	9 ± 4	56 ± 7	123 ± 18	12 ± 7	118 ± 6	255 ± 23
Endosome-escape efficiency (%) [¶]	1.7 ± 0.4	3.9 ± 0.1	4.3 ± 0.1	3.8 ± 1.2	7.4 ± 0.6	12.8 ± 0.2

[*] All the parameters were measured by quantitative western blotting in HeLa and SW480 cells (2×10^5/well) incubated at 37 °C for 6 hr with the indicated concentrations of the antibody in a 12-well culture plate. The cells were washed twice with the low-pH glycine buffer and then PBS. Cell lysates were diluted with PBS to 12 μl volume containing ~10 μg of total proteins for loading on the SDS-PAGE gel followed by western blot analysis. Standard western blotting was also performed on a known amount (0–4 ng) of the purified antibody loaded on the same gel. The amount of the antibody in cell culture media was also determined by western blotting with serial dilution of culture media (~1:12,500 dilution). All the western blotting exposures were performed under the same conditions for direct comparisons. Band densities were quantified using the ImageJ software. The internalized amount of the antibody was estimated by fitting the band intensity of samples to a standard plot, as described before (refs. *18*, *26*)

[†] The internalized amount and cellular uptake efficiency of the antibody after 6 hr of incubation includes the antibody fraction inside whole cells including endocytotic vesicles and cytosol.

[‡] The intracellular concentration of the antibody was estimated assuming the volume of HeLa and SW480 cells as ~2000 μm^3 (refs. *15*, *18*, *26*).

[§] The cytosolic split-GFP complementation assay was performed on HeLa-SA-GFP1-10 and SW480-SA-GFP1-10 cells, which were incubated with the indicated concentrations of an antibody (RT11-i-GFP11-SBP2 and

inRas37-GFP11-SBP2) at 37 °C for 6 hr, as described in detail in the Methods and in our previous works (refs. *15*, *18*, *26*).

‖ The cytosolic molar concentration was estimated by dividing the cytosolic amount with the cytosolic volume (~1000 μm^3) of HeLa and SW480 cells (refs. *18*, *26*).

¶ The endosomal-escape efficiency was estimated by dividing the cytosolic amount by the internalized amount of the antibody.

Table S4. CRC driver mutations from the CCLE and COSMIC datasets.

Cell line	*KRAS*	*NRAS*	*HRAS*	*EGFR*	*ERBB2*	*ERBB3*	*PIK3CA*	*PTEN*	*BRAF*	*MAP2K1/2*	*APC*	*CTNNB1*	*FGFR1*	*YAP1*
HCC44	G12C	WT	WT	WT	WT	WT	WT	WT	WT	WT	WT	WT	WT	WT
THP-1	WT	G12D	WT	WT	WT	WT	WT	WT	WT	WT	WT	WT	WT	WT
NCI-H747	G13D	WT	WT	E282K	WT	WT	WT	WT	WT	WT	Q161*, Q1429*	WT	WT	WT
SNU-175	A59T	WT	WT	A864V	WT	WT	WT	WT	WT	WT	A199V, R232*, K1454fs, G1499*	WT	WT	WT
SK-MEL-2	WT	Q61R	WT	WT	WT	WT	WT	WT	WT	WT	WT	WT	WT	WT
LS513	G12D	WT	WT	WT	WT	WT	WT	WT	E204V	WT	WT	WT	WT	WT
Calu-6	Q61K	WT	WT	WT	WT	WT	WT	WT	WT	WT	WT	WT	WT	WT
H441	G12V	WT	WT	WT	WT	WT	WT	WT	WT	WT	WT	WT	WT	WT
SW620	G12V	WT	WT	WT	WT	WT	WT	WT	WT	WT	Q1338*	WT	WT	WT
HCC2108	Q61H	WT	WT	WT	WT	WT	WT	WT	WT	WT	WT	WT	WT	WT
SW1116	G12A	WT	WT	WT	WT	WT	WT	WT	WT	WT	Q264*, Q1429fs	WT	WT	WT
T24	WT	WT	G12V	WT	WT	WT	WT	WT	WT	WT	WT	WT	WT	WT
SW480	G12V	WT	WT	WT	WT	WT	WT	WT	WT	WT	Q1338*	WT	WT	WT
SK-LU-1	G12D	WT	WT	WT	WT	WT	WT	WT	WT	WT	WT	WT	WT	WT
LS1034	A146T	WT	WT	WT	WT	WT	WT	WT	WT	WT	I1307fs	WT	WT	WT
A549	G12S	WT	WT	WT	WT	WT	WT	WT	WT	WT	WT	WT	WT	WT
LoVo	G13D	WT	WT	WT	WT	WT	WT	WT	WT	WT	R1114*, T1430fs, R2816Q	WT	WT	WT
DLD-1	G13D	WT	WT	WT	WT	N126K, R667H, P1142H	E545K, D549N	WT	WT	WT	R727M, K993N, R2166*, I1417fs	WT	A268S	I246F
H1792	G12C	WT	WT	WT	WT	V104_R106del	WT	WT	WT	WT	WT	WT	WT	WT
SNU-1033	G12D	WT	WT	WT	WT	WT	WT	WT	WT	WT	K1030*	WT	WT	WT
Hs578T	WT	WT	G12D	WT	WT	WT	WT	WT	WT	WT	WT	WT	WT	WT
H1299	WT	Q61K	WT	WT	WT	WT	WT	WT	WT	WT	WT	WT	WT	WT
H2030	G12C	WT	WT	WT	WT	WT	WT	WT	WT	WT	WT	WT	WT	WT
SW403	G12V	WT	WT	WT	WT	WT	Q546K	WT	WT	WT	N125K, F1197fs, S1278*	WT	WT	WT
SNU-81	A146T	E132K	WT	WT	WT	WT	R770Q	R130Q, R233Q, E299*	WT	WT	L360*, S1392*, R1450*, R2204*	E334K, R474Q	A320V	R161*, E324K
SNU-61	G12D	WT	WT	WT	S1050L	WT	WT	WT	WT	WT	R1450*	WT	WT	WT
HCT15	G13D	WT	WT	WT	WT	N126K, R667H, P1142H	E545K, D549N	WT	WT	WT	R727M, K993N, G1416fs, K1561N, R2166*, E2550Q	WT	A268S	I246F
SNU-C2A	G12D	WT	WT	R165Q	R678Q	WT	D725G	3'UTR del	WT	C211Y (MAP2K2)	P2048fs	WT	WT	WT
H460	Q61H	WT	WT	WT	WT	WT	E545K	WT	WT	Y134C (MAP2K1)	WT	WT	WT	WT
HCT116	G13D	WT	WT	WT	WT	Q261*	H1047R	WT	WT	WT	WT	S45del	A343V	WT
HCT8	G13D	WT	WT	WT	WT	N126K, R667H	E545K, D549N	WT	WT	WT	R216*, K993N, R727M, I1417fs	V79I	A268S	WT
LS174T	G12D	WT	WT	WT	WT	WT	H1047R	WT	WT	WT	WT	S45F	E592G	WT
H358	G12C	WT	WT	WT	WT	WT	Q921*	WT	WT	WT	WT	T75A	R209H	WT
H2009	G12A	WT	WT	WT	WT	WT	WT	WT	WT	WT	WT	WT	WT	WT
SNU-407	G12D	WT	WT	V292M	WT	V104M, P262H	H1047R	WT	R726C	WT	WT	T41A	WT	WT
Calu-1	G12C	WT	WT	WT	WT	WT	WT	WT	WT	WT	R1171C	WT	WT	WT
H522	WT	WT	WT	WT	WT	WT	WT	WT	WT	WT	WT	WT	WT	WT
HT29	WT	WT	WT	WT	WT	WT	WT	WT	V600E	WT	E853*, T1556fs	WT	WT	WT
H1650	WT	WT	WT	E746_A750del	WT	WT	WT	WT	WT	WT	A1358T	WT	WT	WT
Colo320DM	WT	WT	WT	WT	WT	WT	WT	WT	WT	WT	S811*	WT	WT	WT
Caco2	WT	WT	WT	WT	WT	WT	WT	WT	WT	WT	Q1337*	G245A	WT	WT
Calu-3	WT	WT	WT	WT	WT	WT	WT	WT	WT	WT	WT	WT	WT	WT
SNU-503	WT	WT	WT	WT	WT	WT	WT	WT	WT	WT	K1543*	WT	WT	WT
HCC827	WT	WT	WT	E746_A750del	WT	WT	WT	WT	WT	WT	WT	WT	WT	WT

Sensitivity to inRas37

- Sensitive
- Resistant
- Resistant (RAS wild-type)

Genetic alteration

- Pathogenic mutant
- Nonpathogenic mutant or wild-type

Table S5. List of resources (antibodies, recombinant proteins, and chemicals) used in this study.

Antibodies or Reagents	Company	Catalog no.
Antibodies		
Rabbit polyclonal anti-MEK1/2	Cell Signaling Technology	Cat. # 9122, RRID: AB_823567
Rabbit polyclonal anti-phospho-MEK1/2 (Ser217/Ser221)	Cell Signaling Technology	Cat. # 9121, RRID: AB_331648
Rabbit monoclonal anti-ERK1/2	Cell Signaling Technology	Cat. # 4695, RRID: AB_390779
Rabbit monoclonal anti-phospho-ERK1/2 (Thr202/Tyr204)	Cell Signaling Technology	Cat. # 4377, RRID: AB_331775
Rabbit polyclonal anti-AKT	Cell Signaling Technology	Cat. # 9272, RRID: AB_329827
Rabbit monoclonal anti-phospho-AKT (Ser473)	Cell Signaling Technology	Cat. # 4060, RRID: AB_2315049
Rabbit polyclonal anti-p70S6K	Cell Signaling Technology	Cat. # 9202, RRID: AB_331676
Rabbit polyclonal anti-phospho-p70S6K (Thr389)	Cell Signaling Technology	Cat. # 9205, RRID: AB_330944
Rabbit polyclonal anti-YAP1	Cell Signaling Technology	Cat. # 4912, RRID: AB_2218911
Rabbit monoclonal anti-Rab5	Cell Signaling Technology	Cat. # 3547, RRID: AB_2300649
Rabbit polyclonal anti-phospho-FOS (Thr325)	Abcam	Cat. # ab27793, RRID: AB_471132
Rabbit monoclonal anti-RAS	Abcam	Cat. # ab108602, RRID: AB_10891004
Rabbit polyclonal phospho-ERK1/2 (Thr202/Tyr204)	Abcam	Cat. # ab4819, RRID: AB_304655
Rabbit polyclonal anti-Ki-67	Abcam	Cat. # ab15580, RRID: AB_443209
Mouse monoclonal anti-KRAS	Santa Cruz Biotechnology	Cat. # sc-30, RRID: AB_627865
Mouse monoclonal anti-β-actin	Santa Cruz Biotechnology	Cat. # sc-69879, RRID: AB_1119529
Donkey polyclonal anti-goat IgG antibody, HRP-conjugated	Santa Cruz Biotechnology	Cat. # sc-2033, RRID: AB_631729
Rabbit polyclonal anti-mouse IgG antibody, HRP-conjugated	Sigma-Aldrich	Cat. # A9044, RRID: AB_258431
Goat polyclonal anti-rabbit IgG antibody, HRP-conjugated	Sigma-Aldrich	Cat. # A6154, RRID: AB_258284
Mouse monoclonal anti-GST, HRP-conjugated	Sigma-Aldrich	Cat. # A7340, RRID: AB_258340
Mouse monoclonal anti-polyHistidine, HRP-conjugated	Sigma-Aldrich	Cat. # A7058, RRID: AB_258326
Mouse monoclonal anti-FLAG	Sigma-Aldrich	Cat. # F3165; RRID: AB_259529
Goat polyclonal anti-human IgG antibody (Fab specific)	Sigma-Aldrich	Cat. # I5260, RRID: AB_260206
Goat polyclonal anti-rabbit IgG antibody, TRITC-conjugated	Sigma-Aldrich	Cat. # T6778, RRID: AB_261740
Mouse monoclonal anti-human integrin αvβ3	R&D Systems	Cat. # MAB3050, RRID: AB_2128187
Mouse monoclonal anti-human integrin αvβ5	R&D Systems	Cat. # MAB2528, RRID: AB_2280706
Goat polyclonal anti-human IgG antibody (Fc specific)	Invitrogen	Cat. # 31125, RRID: AB_429669
Goat polyclonal anti-human IgG antibody, HRP-conjugated	Invitrogen	Cat. # 62-8420, RRID: AB_2533962
Goat polyclonal anti-human IgG antibody, Alexa Fluor 488-conjugated	Invitrogen	Cat. # A-11013; RRID: AB_141360
Goat polyclonal anti-mouse IgG antibody, Alexa Fluor 488-conjugated	Invitrogen	Cat. # A-11001, RRID: AB_2534069
Goat polyclonal anti-rabbit IgG antibody, Alexa Fluor 488-conjugated	Invitrogen	Cat. # A-11008, RRID: AB_143165
Mouse monoclonal anti-c-Myc	Invitrogen	Cat. # MA1-980, RRID: AB_2537627
Rat monoclonal anti-HA, HRP-conjugated	Roche	Cat. # 12013819001, RRID: AB_390917
Chemicals and Recombinant Proteins		
Human integrin αvβ5	R&D Systems	Cat. # 2528-AV-050
Human integrin αvβ3	R&D Systems	Cat. # 3050-AV-050
Human EGF	Thermo Fisher Scientific	Cat. # PHG0311L
Trametinib	Selleck Chemicals	Cat. # S2673, CAS # 871700-17-3
LY294002	Merck Millipore	Cat. # 440202, CAS # 154447-36-6
Copanlisib	Adooq Bioscience	Cat. # A11766, CAS # 1032568-63-0
Afatinib	Selleck Chemicals	Cat. # S1011, CAS # 439081-18-2
Ponatinib	Selleck Chemicals	Cat. # S1490, CAS # 943319-70-8
iCRT14	Sigma-Aldrich	Cat. # SML0203, CAS # 677331-12-3
Verteporfin	Sigma-Aldrich	Cat. # SML0534, CAS # 129497-78-5
GppNHp	Sigma-Aldrich	Cat. # G0635, CAS # 148892-91-5
GDP	Merck Millipore	Cat. # 20-177
EZ-Link Sulfo-NHS-Biotin	Thermo Fisher Scientific	Cat. # 21217, CAS # 119616-38-5
Sephadex G-25 in PD-10 desalting column	GE Healthcare	Cat. # 17085101
Superdex 200 10/300 GL column	GE Healthcare	Cat. # 17-5175-01
Zenix SEC-300 column	Sepax Technologies	Cat. # 213300-7830
Streptavidin-conjugated R-phycoerythrin (SA-PE)	Thermo Fisher Scientific	Cat. # S21388
TMB-ELISA solution	Thermo Fisher Scientific	Cat. # 34028
Halt Protease Inhibitor Cocktail	Thermo Fisher Scientific	Cat. # 78440
Fluorescence Mounting Medium	Dako	Cat. # 3023
Raf-1 RBD, agarose	Merck Millipore	Cat. # 14-278
Lipofectamine RNAiMAX	Invitrogen	Cat. # 13778075
Lipofectamine 3000	Invitrogen	Cat. # L3000008
Matrigel Basement Membrane Matrix	Corning	Cat. # 354234
Isoflurane	Piramal Critical Care	Cat. # 66794-017-25

Poly-L-lysine solution	Sigma	Cat. # P8920
Cardiolipin	Sigma	Cat. # C0563
Hemocyanin (KHL)	Sigma	Cat. # H8283
Deoxyribonucleic acid (dsDNA)	Sigma	Cat. # D4522
Insulin	Sigma	Cat. # I9278
siRNA targeting human integrin β5 #1	Bioneer	Cat. # 1075906
siRNA targeting human integrin β5 #2	Bioneer	Cat. # 1075915